ARTICLE

Modeling the Water–Bioglass Interface by Ab Initio Molecular Dynamics Simulations

Antonio Tilocca*,† and Alastair N. Cormack‡

Department of Chemistry, University College London, London, U.K., and New York State College of Ceramics, Alfred University, Alfred, New York 14802

ABSTRACT The hydration of the surface of a highly bioactive silicate glass was modeled using ab initio (Car–Parrinello) molecular dynamics (CPMD) simulations, focusing on the structural and chemical modifications taking place at the glass–water interface immediately after contact and on the way in which they can affect the bioactivity of these materials. The adsorption of a water dimer and trimer on the dry surface was studied first, followed by the extended interface between the glass and liquid water. The CPMD trajectories provide atomistic insight into the initial stages relevant to the biological activity of these materials: following contact of the glass with an aqueous (physiological) medium, the initial enrichment of the surface region in Na^+ cations establishes dominant Na^+–water interactions at the surface, which allow water molecules to penetrate into the open glass network and start its partial dissolution. The model of a Na/H-exchanged interface shows that Ca^{2+}–water interactions are mainly established *after* the dominant fraction of Na is leached into the solution. Another critical role of modifier cations was highlighted: they provide the Lewis acidity necessary to neutralize OH^- produced by water dissociation and protonation of nonbridging oxygen (NBO) surface sites. The CPMD simulations also highlighted an alternative, proton-hopping mechanism by which the same process can take place in the liquid water film. The main features of the bioactive glass surface immediately after contact with an aqueous medium, as emerged from the simulations, are (a) silanol groups formed by either water dissociation at undercoordinated Si sites or direct protonation of NBOs, (b) OH^- groups generally stabilized by modifier cations and coupled with the protonated NBOs, and (c) small rings, relatively stable and unopened even after exposure to liquid water. The possible role and effect of these sites in the bioactive process are discussed.

KEYWORDS: surface structure • surface reactivity • bioactive glasses • silicate glasses • glass surface • liquid water • density functional theory • molecular dynamics simulations • Car–Parrinello

1. INTRODUCTION

Surface-active multicomponent silicate glasses such as 45S5 Bioglass(R) represent the core component of many current biomaterials with applications in biomedicine and tissue engineering, where a bioglass-based device promotes growth, healing, and repair of damaged/deteriorated tissues (1–6). Most applications exploit the ability of the glass to combine with soft and hard living tissues, which leads to high biocompatibility and efficient integration of the biomaterial with the host (7). Contact of a bioactive glass (BG) with physiological fluids leads to a sequence of rapid chemical steps, which result in the crystallization of bonelike hydroxyapatite (HAp) on the glass surface: the high affinity between living tissues and the HAp layer is the key factor for the success of biomedical applications; as a matter of fact, glass compositions that lack the ability to crystallize HAp in an aqueous environment are bioinactive (6, 7).

The direct correlation established between the rate of HAp crystallization and bioactivity enables one to predict the suitability of new compositions for biomedical applications, based on in vitro or in vivo trial-and-error approaches (8–12). At the same time, fundamental studies of the basic interactions leading to HAp formation are highly needed to support further progress in this field; the sequence of the physicochemical steps following immersion of the glass in body fluids has been roughly identified (6, 7): the bioactive process initially involves partial dissolution of the glass through ion exchange with the solution, hydrolysis of Si–O–Si bridges, and release of soluble silicate units (1). Unlike other fully resorbable biomaterials (13), the dissolution of silicate bioglasses is limited to their surface and does not progress further to the bulk: therefore, a stable interfacial region is maintained for the critical time during which additional chemical stages can lead to HAp deposition and bonding to tissues (6, 14). Whereas these processes and features are common to all BGs, a clear understanding of the way in which they reflect different structural and chemical properties of different glass compositions still has to emerge: wide changes in the rate of HAp deposition result from small changes in the glass composition (1), but the critical relationships between composition and bioactivity, for instance, in terms of the particular structural features that enhance/inhibit one or more stages of the bioactive mechanism, are mostly unknown. The identification of structural markers of bioactivity would enable systematic optimization of the chemical and mechanical properties of the glass targeted for biomedical applications: nevertheless, the intrinsic difficulty to obtain accurate data on the atomistic structure of these multicomponent amorphous materials has

* Corresponding author. E-mail: a.tilocca@ucl.ac.uk.
Received for review March 23, 2009 and accepted May 14, 2009
† University College London.
‡ Alfred University.
DOI: 10.1021/am900198t

Published on Web 06/01/2009

slowed progress in this direction. In recent years, nuclear magnetic resonance (15, 16), neutron diffraction (17, 18) and molecular dynamics (MD) simulation techniques (19−26) have led to promising advances in the determination of *bulk* structural features related to the biological activity of silicate and phosphate glasses. Traditional, melt-derived BGs contain a low silica fraction and a corresponding high fraction of network-modifier cations such as Na^+ and Ca^+, which break Si−O−Si bridges, creating nonbridging O atoms (NBOs) and opening (depolymerizing) the glass network (27). The substantial network fragmentation of low silica compositions, with significant concentrations of weakly bound phosphosilicate chains, promotes fast initial dissolution of the glass and leads to high bioactivity (21, 22); on the other hand, segregation of nanoscale inhomogeneities and separation of calcium phosphate nanodomains in the bulk has a clear inhibitor effect on the bioactivity of higher-silica BGs (24, 26). These general effects were indirectly inferred by comparing the bulk structures of glasses of known different bioactivity; a further substantial step forward can be taken by shifting the focus of investigations *directly* onto the interface between the amorphous phase and the surrounding medium, that is, on the crucial region where the particular structural features of BGs come into play and determine their special biological activity. While experimental surface-analytical methods are essential to highlight the transformations occurring after contact of the BG with a physiological solution (5, 28, 29), the interpretation of these changes is often not straightfoward, given the high heterogeneity of the surface of BGs, exposing many sites of different strength and geometry. In fact, the complexity of the BG surface makes it significantly harder to investigate, compared not only to crystalline oxides but also to other amorphous surfaces such as pure silica (30, 31). Molecular simulations represent a fundamental tool to probe these systems with atomistic resolution, aiding the interpretation of experimental data and providing new insight: in the case of BG surfaces, the complexity of the atomic environments and of the rapid chemical transformations occurring there upon contact with an aqueous solution demands the use of parameter-free ab initio methods (32) to describe these systems with high accuracy. We have recently applied Car−Parrinello (CP) (33) ab initio MD simulations (32) and density functional theory (DFT) energy minimizations to model the as-created, dry surface of 45S5 Bioglass(R), identifying and characterizing several potential active sites, on the basis of their individual interaction with a water molecule, used as a representative polar probe (34). This powerful (and computationally demanding) approach revealed a number of interesting features: undercoordinated Si centers, formed on the as-created surface, spontaneously dissociate water at room temperature and will be presumably hydroxylated in a fully hydrated sample; water is also attracted to Lewis acids such as Na^+ and Ca^{2+} cations, which populate the as-created BG surface in significant amounts. Perhaps the most surprising finding of these simulations was the low affinity of water for small rings, comprising two or three silicate units, which also represent common structural features of BG and silica surfaces (35−38). The CPMD-DFT calculations clearly highlighted that, despite their internal strain, opening of these rings through water adsorption and dissociation is hindered by a significant energy barrier (0.62 eV), possibly in connection with the presence of alternative, more favorable water adsorption sites such as the Lewis acids mentioned before (34). This finding is quite relevant in the context of the bioactive mechanism because small rings have often been proposed as possible nucleation sites for HAp (36−38); therefore, the previous simulations seem to support this idea, providing a sound explanation for the stability/availability of these sites on the glass surface even after exposure to aqueous media. A potential limit of these simulations was that a single, isolated molecular probe had been employed to look at the activity of the individual sites: while this is a convenient and well-established approach to selectively and reproducibly investigate the properties of oxide surfaces in situ (39−41), it is also well established that cooperative effects can reduce the activation barrier for processes involving water adsorption and dissociation at oxide surfaces (42−44) and at 2M rings in particular (45). Therefore, new critical steps involve modeling of the effect of intermolecular (water−water) interactions on the water−BG interface. Besides studying higher coverages of interacting water molecules adsorbed on the surface (39), the final target is the actual interface formed in biomedical applications: that is, the glass in contact with a *bulk* liquid water solvent. An atomistic model of this interface enables a closer assessment of the hydrophobic/hydrophilic nature of the individual sites identified on the dry surface and provides a realistic picture of the BG surface immediately after immersion in body fluids.

In this work, we present large-scale CPMD simulations of the 45S5 Bioglass(R)−water interface, starting from an adsorbed water dimer and trimer and then moving to a liquid water film; a model of the ion-exchanged surface in contact with a water film completes the calculations. These simulations represent one of the first direct attempts to model a realistic interface between liquid water and a modified silicate glass with first-principles accuracy. They provide new atomistic insight on the way in which water affects the glass durability, which is a major issue not only for the applications of biomaterials based on 45S5 and related compositions but also for corrosion processes, microelectronics (water also affects the properties of optical fibers), and storage of radioactive waste applications (46, 47).

2. DETAILS OF THE SIMULATIONS

2.1. Computational Methods. The CP code embedded in the Quantum-ESPRESSO package (48) was employed in all of the MD simulations. The electronic structure was treated within the generalized gradient approximation to DFT, through the Perdew−Burke−Ernzerhof exchange-correlation functional (49). Vanderbilt ultrasoft pseudopotentials were employed to represent core−valence electron interactions (50), explicitly including Na and Ca semicore

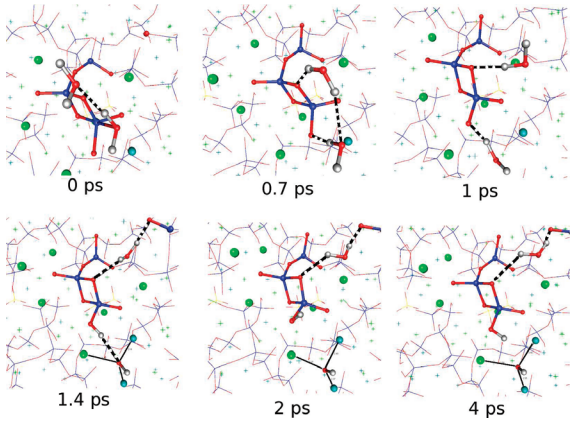

FIGURE 1. Time evolution of a water dimer adsorbed on an exposed 2M ring on the bioglass surface (top view): the atoms involved in the water−ring interaction are highlighted as ball-and-stick, whereas all of the other atoms are represented as wireframe. Dashed lines denote hydrogen bonds. Color code: O, red; H, white; Si, blue; P, yellow; Na, green; Ca, turquoise.

shells in the valence. A plane-wave basis set was used, with cutoffs set to 30 and 240 Ry for the smooth part of the wavefunctions and the augmented charge, respectively; k sampling was restricted to the Γ point. The MD time step δt and fictitious electronic mass μ were 0.17 fs and 700 au, respectively; we used the deuterium mass for H atoms to effectively decouple the electronic from the ionic degrees of freedom, thus allowing a larger μ and a longer δt. This is a well-established computational setup for modeling of water adsorption on the surface of silica (51−53) and of other oxides (54, 55) with CPMD.

2.2. Adsorption of Water Dimer/Trimer: Computational Setup. The initial simulations probed the reactivity of an exposed two-membered (2M) ring, formed by two edge-sharing SiO_4 tetrahedra, toward a group of two or three interacting water molecules, in order to investigate whether cooperative interactions between water molecules affect the stability of the ring sites, with respect to single-water adsorption (34, 44). In these simulations, we extended the 45S5 glass surface model recently obtained in the study of single-water adsorption (34): the surface was represented by a slab including 122 atoms, with a vertical separation (vacuum) of ∼10 Å between periodic images. Water was adsorbed on the top face of the slab only, and the atoms in the bottom 3−4 Å of the slab were fixed to their bulk positions (see ref 34 for further details). Starting from the slab model obtained in our previous work (34), a pair of water molecules was arranged on top of a 2M ring in the same surface, as shown in Figure 1. The dynamic evolution of this configuration was then followed through a CPMD trajectory at 300 K; another CPMD run at the same temperature was started after the addition of a third water to a configuration extracted from the dimer trajectory, as shown in Figure 2. Both CPMD trajectories were terminated after all of the water molecules settled in relatively stable configurations, which required 4 ps for the dimer and 16 ps for the trimer.

2.3. Glass−Liquid Water Interface: Computational Setup. Some changes to the general setup of the

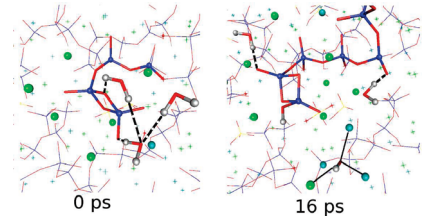

FIGURE 2. Top view of a water trimer adsorbed on an exposed 2M ring on the bioglass surface: the atoms involved in the water−ring interaction are highlighted as ball-and-stick, whereas all of the other atoms are represented as wireframe. Dashed lines denote hydrogen bonds. Color code: O, red; H, white; Si, blue; P, yellow; Na, green; Ca, turquoise. The initial (0 ps) and final (16 ps) configurations of the MD trajectory are shown.

calculations were needed in order to model a BG surface in contact with a liquid water film: a larger slab was generated from scratch, in order to provide a higher surface area in contact with an extended liquid sample. Following the same general procedure recently refined to model bioactive silicate glasses (23, 34), a relatively large model of bulk 45S5 Bioglass(R) was generated first by using CPMD to melt-and-quench from 3000 to 300 K an initial mixture of the appropriate composition 45.7:24.3:27.1:2.9 mol % SiO_2/Na_2O/CaO/P_2O_5; this was obtained by randomly inserting 32 SiO_2, 17 Na_2O, 19 CaO, and 2 P_2O_5 units in a periodic cubic box of a = 13.925 Å side; the system included 199 atoms and 1304 electrons in total. The equilibrated sample of the bulk glass was then used to generate a free surface, by cutting a slab from the bulk following the procedure outlined below.

In order to obtain a model of the dry surface, a slab geometry was created by increasing the c parameter of the volume-optimized supercell by 10 Å: with three-dimensional periodic boundary conditions, this leads to a corresponding vacuum region separating the top face of the slab from the periodic image of the bottom face. As for the runs with isolated water dimer and trimer, the atoms in the bottom part of the slab were fixed to their bulklike positions, and the analysis was focused on the interaction of water with the top side of the slab only. The latter choice is dictated by the particular features of the surface region of our system: if *both* (top and bottom) exposed faces of the slab were to be fully relaxed, they should be separated by a bulklike region of sufficient (at least a few angstroms) thickness in the central portion of the slab. While this requirement can be achieved in ab initio slab models of crystalline and amorphous SiO_2 (56), a much thicker slab than computationally affordable would be required to attain a bulk region separating two exposed BG surfaces: in this case, it is preferable to relax one face of the slab only and preserve bulklike effects by fixing the atoms at the bottom of the slab to their initial (bulk glass) positions (57, 58). The fraction of water molecules in close contact with the unrelaxed surface are not considered in the statistical analysis of the MD trajectories; the overall thickness of the water film (>10 Å) ensures that the remaining water molecules closer to the fully relaxed top surface represent a reliable sample of interfacial liquid water.

The as-created dry slab cut from the bulk was relaxed in a CPMD trajectory of 3 ps at 300 K, followed by annealing to 600 K for an additional 5 ps. Then, a film of 52 water molecules, extracted from a liquid sample equilibrated with CPMD within the same theoretical framework, was then inserted in the vacuum region. Care was taken to further adjust the cell parameter c to avoid unphysically short initial contacts between the atoms of the surface and those of the water molecules; the final value ($c = 25.2$ Å) roughly corresponds to a minimum distance of 2 Å separating a molecule in the water film from the closest surface atom; the water molecules fill up this empty space quickly after the start of the MD run. The hydrated system contained 355 atoms and 1720 electrons in total. A CPMD trajectory of ~5 ps without temperature control was then carried out, followed by a room temperature production run of another 5 ps. Statistical analysis was carried out on the room temperature data only.

In order to mimick the effect of the Na^+-H^+ exchange process that follows hydration of the surface, the last configuration of the CPMD run with the hydrated slab was modified by replacing all Na^+ ions in the top layers of the surface (seven in total) with a proton; an 8 ps MD run without temperature control was then carried out, followed by a final 6 ps trajectory at room temperature.

3. RESULTS

3.1. Adsorption of Water Dimer and Trimer. The starting configuration with an adsorbed water dimer, labeled "0 ps" in Figure 1, involved a water molecule interacting with one of the two Si of a 2M ring and donating a hydrogen bond (Hb) to the second water molecule, located above the exposed bridging oxygen (BO) of the same 2M ring. In the initial stages of the dynamics, the Hb pattern connecting the two molecules to each other and to the surface is relaxed, and an extended 4M ring is formed (0.7 ps), involving the water dimer and two O atoms belonging to the 2M ring. However, this arrangement is rapidly broken as the two molecules separate (1 ps), while still individually interacting with the ring through Hb's. After 1.4 ps, a water molecule partially dissociates, donating a proton to a ring NBO along the Hb that connected them; closer inspection of the MD configurations highlights that this process is triggered by the simultaneous contact with two modifier cations (an Na^+ and a Ca^{2+}, visibile in the panel) with the water molecule; in other words, the dissociation starts as soon as the second cation enters the water coordination shell: this same feature was also observed in other water dissociation events (see section 3.2). The resulting hydroxyl is further stabilized by coordination of a third Ca^{2+} cation: the arrangement highlighted in the right bottom side of the 1.4 ps panel, with the OH^- lying at the center of the triangle formed by the three modifier cations, is stable for the rest of the MD trajectory (4 ps). At the same time, the second water molecule also reaches a stable configuration, bridging between the central BO of the ring and an NBO belonging to another portion of the surface. The evolution of the MD trajectory indicates that the interaction of a water dimer with an exposed 2M ring can lead to water dissociation, provided that Na^+ and Ca^+ network-modifier cations are available nearby to trigger the proton transfer to an NBO and stabilize the remaining hydroxyl group; while the interaction of an isolated water monomer with small rings on the BG surface was found to be rather weak and desorption of the monomer was observed in some cases (34), the presence of a second molecule interacting with the same ring site seems to strengthen the water–ring interaction with respect to the monomer, and the two molecules always remain bound to the surface during the room temperature trajectory. Nonetheless, neither this somewhat stronger water–surface interaction nor the collective action of two water molecules creating alternative reaction paths (42, 60) (see also below) are sufficient to overcome the kinetic barrier associated with opening of the 2M ring (34), which remains unopened. This situation does not change with participation of a third molecule: the initial trimer configuration (labeled "0 ps" in Figure 2) was obtained by the addition of a third molecule to the hydrogen-bonded dimer configuration 0.7 ps in Figure 1. The dynamical evolution of the trimer is rather similar to that of the dimer case: in particular, one molecule dissociates and forms a hydroxyl group again encaged within three cations, in a rather stable configuration: the trajectory was extended up to 16 ps in the trimer case. Regarding the two other molecules, one remains hydrogen-bonded to the 2M ring, whereas the other one moves slightly apart, still remaining hydrogen-bonded to another exposed NBO on the surface. The main point highlighted by these MD runs is that the 2M-ring site is rather (kinetically) stable, and the collective action of up to three water molecules does not create a favorable pathway for ring opening, in agreement with recent quantum-mechanical calculations that showed a significant barrier to ring opening even in the presence of three molecules (45). This could reflect the fact that, in both dimer and trimer cases, configurations where the water molecules simultaneously interact with each other *and* with the ring appear less stable than configurations where the molecules *individually* interact with the ring, with no direct water–water interaction, possibly because of the small size of the 2M ring, which cannot easily accommodate two interacting water molecules. Therefore, additional reaction pathways involving several water molecules, with lower-energy transition states stabilized by intermolecular Hb's (42, 44, 60), are not easily accessed in this case, and water dissociation at small ring sites is more likely to occur *without* ring opening, leading to a partially hydroxylated ring site, which could represent an important intermediate in the bioactive mechanism.

3.2. Glass–Liquid Water Interface. The as-created glass surface (which here and in the following refers to the fully relaxed, top face of the slab obtained from the large bulk glass; see section 2.3) initially exposed two undercoordinated network-forming atoms: Si_{3c} and P_{3c}. Both of these defects were rapidly healed upon relaxation, through formation of an Si–O–P link incorporated in a 2M ring; another 2M ring with two edge-sharing Si tetrahedra was also exposed on the relaxed surface.

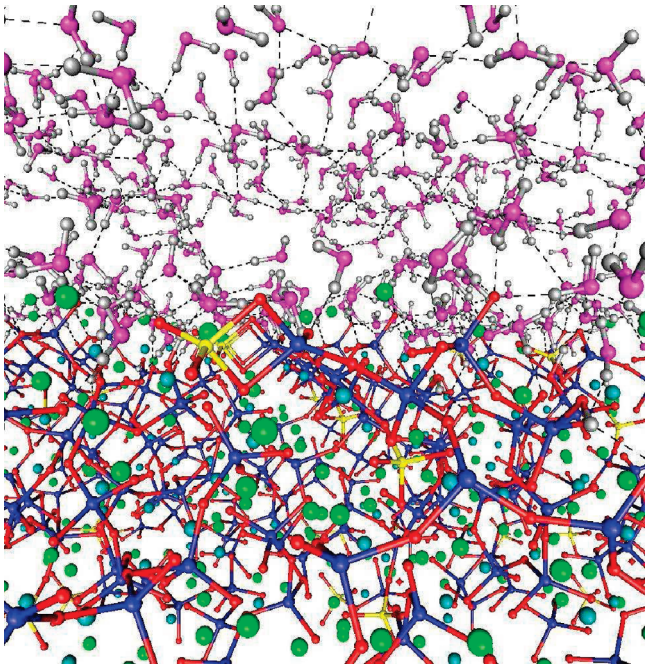

FIGURE 3. Side view of the (periodically repeated) glass−water interface. Color code: red, O_{glass}; purple, O_{water}; white, H; blue, Si; green, Na; turquoise, Ca.

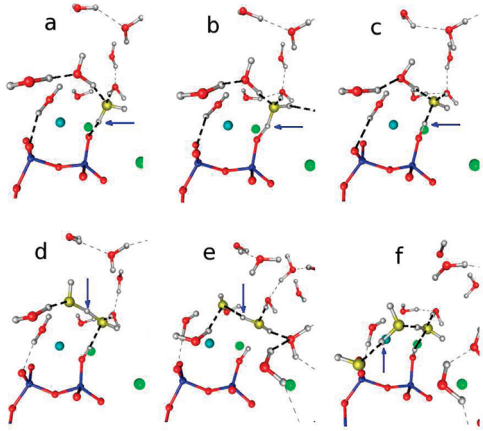

FIGURE 4. Water dissociation mechanism at the glass−water interface. Only the atoms closest to the dissociation site are shown. Color code: red, O; white, H; blue, Si; green, Na; turquoise, Ca. The water molecules involved in the proton-transfer chain are highlighted in yellow. Bold dashed lines highlight hydrogen bonds relevant to the proton hopping and dissociation discussed in the text, whereas other Hb's are marked by dashed thin lines. The blue arrow highlights the tranferred protons.

The relaxed dry surface was then put in contact with a film of liquid water as described in section 2.3. A side view of the hydrated surface is shown in Figure 3. During the first 2 ps of the MD trajectory, a water molecule dissociates at a surface NBO site, through the sequence of proton transfers illustrated in Figure 4, where the dissociating water molecule(s) and the subsequent proton jumps are highlighted. The first H-transfer (panels a−c) takes place along the Hb linking the central water molecule to the exposed Si-NBO. The remaining OH^- is initially encaged in a shell of three Hb's donated by adjacent molecules (panel c), before being converted back to molecular water through a proton hopping from an adjacent water molecule along one of the three Hb's (panels d and e). The latter transfer creates a new OH^- (panel e), which, in turn, accepts a proton from yet another adjacent water (panel f). The chain of proton hoppings between water molecules highlighted in Figure 4 essentially shifts the initial OH^- "defect" from the initial dissociation site at the surface to another region of the water film. Following this first reaction, a second water dissociation at a glass NBO occurs after 3.5 ps from the beginning of the trajectory (not shown), with a similar proton-hopping mechanism involving few water molecules; in this case, the sequence of consecutive proton transfers is interrupted when the resulting hydroxyl is stabilized by close contacts with three modifier cations (one Ca^{2+} and two Na^+) in an arrangement similar to the final one in Figures 1 and 2 for the water dimer and trimer, respectively. As for the water dimer case, closer inspection of the trajectory confirms that short-distance contacts with *two* Na/Ca cations and an NBO triggers dissociation of the water molecule, which can transfer a hydrogen to the NBO either directly or indirectly (through proton hopping along other water molecules). A third cation approaches and completes coordination of the resulting OH^- shortly afterward: the $M^{n+}\cdots OH$ interactions gradually replace $H\cdots OH$ water−water Hb's, and the resulting M−OH adducts remain bound for the remaining length of the MD trajectory. The same is true for the Si−NBO−H silanols, whereas no further water dissociations are observed in the trajectory.

Neither of the two small rings was opened throughout the CPMD trajectory; the simulations show that exposed NBOs appear as more reactive basic sites, able to extract a proton and dissociate water molecules, provided that additional acidic sites are available to stabilize the resulting OH^-. In addition to undercoordinated Si (34) and network-modifier cations, whose effectiveness as acidic sites was already revealed by their interaction with small gas-phase water clusters discussed before, liquid water also enables hydroxylation of surface NBOs by stabilizing the resulting OH^- through proton hopping along water chains.

The distribution (z profile) of the atomic species along the surface normal is shown in Figure 5a. The changes in the profile of all species for $z > 5$ Å allow us to identify the surface region of the slab as the top 5−6 Å ($5 < z < 10$ Å), whereas only water populates the region above $z \sim 10$ Å. The most prominent features are the significant penetration of water within the surface region, and the net predominance of Na^+ over the other cationic species in this region: in particular, a drop in the Ca^{2+} fraction with respect to the bulk glass is observed approaching the glass surface, with a corresponding increase in the Na^+ fraction.

In order to examine the structure of the water film in detail, the water density (61) was plotted as a function of the vertical distance from the surface (Figure 5b); the dashed vertical guidelines reveal that the initial band corresponds to water in direct contact and partially inside the glass surface ($5 < z < 10$ Å), which in the following will be labeled DHW, for "direct hydration water". The region immediately above ($10 < z < 15$ Å), which panel a in the figure reveals to

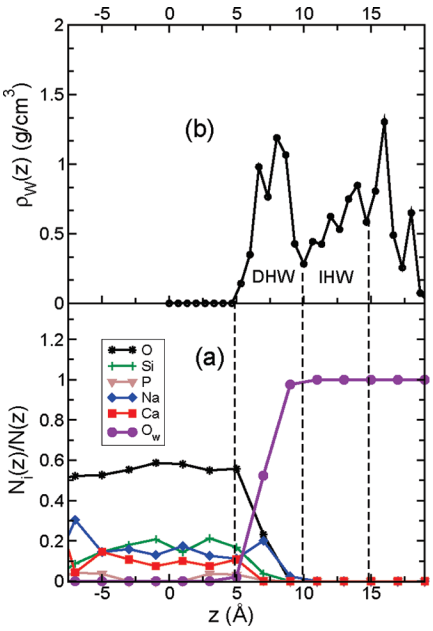

FIGURE 5. (a) z profiles of the fraction of O_w, O, Si, P, Na, and Ca atoms (where O_w and O denote O atoms belonging to water or to the glass, respectively) in the glass−liquid water interface model: the simulation box was divided into slices 2 Å thick along z, and the number of atoms found in each slice was averaged over the corresponding MD trajectory; the atomic fraction N_i/N in each z slice is plotted, where N_i is the average number of atoms of species i and N is the average total number of atoms of all species found in the slice; $z = 0$ corresponds to the center of the slab. (b) Density distribution of water molecules along the vertical direction from the surface: the approximate density $\rho_w(z)$ is calculated from the $N_w(z)$ average number of water molecules in the slice centered at height z and the corresponding volume of each slice.

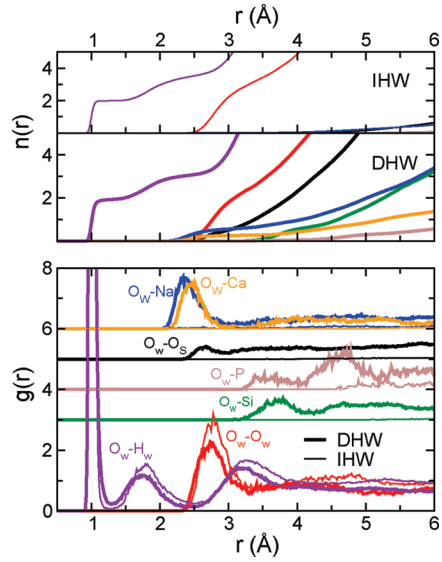

FIGURE 6. (bottom panel) Intermolecular rdf's for the interaction of water oxygen atoms O_w with O_w and H_w, as well as with O, Si, Na, Ca, and P species of the glass. The rdf's for water molecules in direct contact with the surface (DHW, bold curves) and for those immediately above (IHW, thin curves) are plotted separately. Note that molecules closer to the surface are less likely to be surrounded by an isotropic bulk water environment at large distances, hence, the nonunit asymptotic limit for large r separations in the water−water $g(r)$'s in the DHW region. Curves are shifted vertically for clarity. (central and top panels) Cumulative coordination numbers $n(r)$, integrals of the corresponding rdf's in the bottom panel. The central panel shows the $n(r)$'s for water molecules in close contact with the surface (DHW region), whereas the top panel concerns the IHW molecules in the region immediately above.

be occupied by water only, will be labeled "indirect hydration water" (IHW), as these molecules are not directly bound to the surface.

The structural features of water molecules belonging to the DHW and IHW regions are analyzed through the corresponding radial distribution functions (rdf's), calculated separately for molecules in each region. The rdf's in the bottom panel of Figure 6 highlight strong water−water Hb's not only in the pure-water IHW region but also in the DHW layer: actually, the O_w−O_w and O_w−H_w peak distances, despite some statistical noise, denote stronger Hb's formed between water molecules in direct contact with the surface: going from IHW to DHW, $R_{O_w-O_w}$ decreases from 2.76 to 2.71 Å and $R_{O_w-H_w}$ decreases from 1.79 to 1.74 Å.

The main interactions involving water molecules in the DHW region, in addition to Hb's with each other, are with Na^+ and Ca^{2+} cations, with O_w−Na and O_w−Ca peaks centered at 2.34 and 2.45 Å, respectively, close to the cation−oxygen distances in the bulk glass (19). Even though Figure 5a showed that Si atoms are present in the same region, water molecules appear to interact only weakly with them, with a broad Si−O_w peak centered around 3.7 Å, reflecting the intrinsic hydrophobicity of siloxane bonds at defect-free silica surfaces (52); similar considerations apply to the water−phosphorus interaction, with an O_w−P peak around 3.6 Å. Finally, Hb's between water and the exposed oxide ions of the surface are revealed by the small O_w−O_s peak at 2.65 Å. In general, no strong affinity seems to exist between water and the Si, P, and O atoms forming the glass network. No water−substrate interactions involve water molecules in the IHW region, which is dominated by bulklike intermolecular water−water interactions (see below).

The local environment of a water molecule can be further characterized through the cumulative coordination numbers $n(r)$ plotted in the top two panels of Figure 6 for each individual interaction involving water; the average composition of the water coordination shell can be measured using for each interaction the $n(r=R_c)$ coordination number, where R_c is the distance cutoff corresponding to the first minimum of the corresponding rdf in Figure 6. Each water in the DHW region forms 2.5 Hb's with other water molecules (that is, 2 in approximately half of the simulation time and 3 in the remaining time); the O_w−H_w coordination number at the 2.5 Å cutoff, after subtraction of the intramolecular O−H contribution, is 1.15, indicating that the water−water Hb's are equally divided between donor and acceptor. Each water molecule in the DHW region also coordinates 0.6 Na^+, 0.2 Ca^{2+}, and 0.5 surface O atoms, on average. No Si/P species are found within 3.5 Å of a water O atom, confirming their weak mutual affinity. On the basis of this quantitative analysis, the local environment of a water molecule in the DHW region could be summarized as in the snapshot shown in Figure 7: essentially, compared to the tetrahedral network of water−water Hb's surrounding a molecule in bulk liquid water, upon contact with the glass surface, a modifier cation (typically Na^+) takes one of the four sites in the tetrahedral

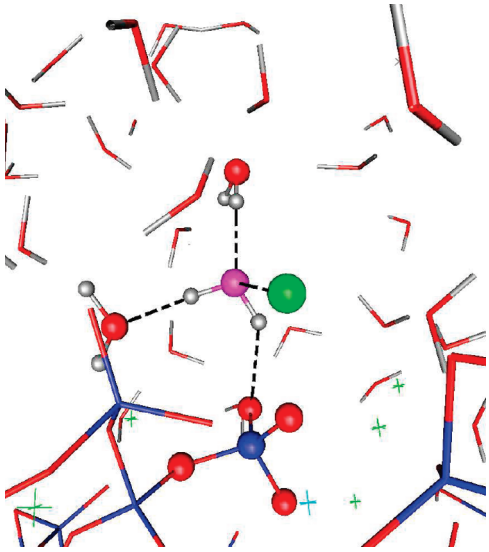

FIGURE 7. Local coordination environment of a water molecule near the glass surface (snapshot extracted from the MD trajectory). The atoms in the coordination shell of the central water molecule (colored purple) are highlighted as spheres. Color code: red, O; white, H; blue, Si; green, Na; turquoise, Ca.

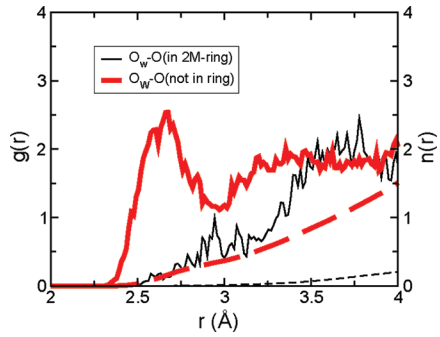

FIGURE 8. O(water)−O(surface) radial and coordination functions, separated into the contributions of surface O atoms incorporated (thin curves) or not incorporated (bold curves) in 2M rings. Dashed lines represent cumulative coordination numbers $n(r)$. All water molecules in the $z < 15$ Å range were taken into account in the analysis.

coordination shell, whereas another site is shared (timewise) between a surface O atom and another water molecule. As we move away from the glass surface, Figure 6 (top panel) shows that water in the IHW region rapidly recovers bulklike character, with each molecule encaged in a coordination shell of 3.5 hydrogen-bonded water molecules, half of which donating/receiving Hb's, with a negligible number of coordinated Na^+ or Ca^{2+}.

The low affinity of liquid water for atoms in the exposed phosphosilicate network also extends to the small ring fragments: this is evident if the water−surface O interaction is split into the interaction of water with O atoms enclosed in 2M rings and with all other exposed O atoms in the glass. Figure 8 denotes a clear preference of water molecules for exposed O atoms not incorporated in a ring, as shown by the Hb peak around 2.66 Å completely absent in the O(water)−O(ring) rdf with a much smaller corresponding coordination number. This shows that the interaction of water molecules with surface O atoms is preferentially oriented toward the O atoms *not* involved in rings.

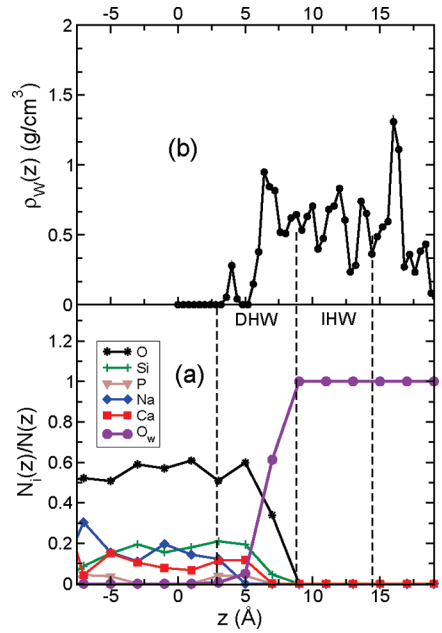

FIGURE 9. (a) z profiles of the fraction of O_w, O, Si, P, Na, and Ca atoms (where O_w and O denote O atoms belonging to water or to the glass, respectively) in the glass−liquid water interface model after Na/H ion exchange. (b) Density distribution of water molecules along the vertical direction from the surface.

3.3. Na^+/H^+-Exchanged Interface. As discussed in section 2.3, in order to model the ion-exchanged surface, a calculation was performed in which all of the Na ions populating the uppermost region of the hydrated glass surface (Figure 5) were replaced with protons, which were then left free to migrate toward a stable arrangement in a relatively long (8 ps) trajectory with no temperature control, followed by an *NVT* run of 5.5 ps at $T = 300$ K. The initial relaxation led to a moderate increase in temperature (up to 550 K), during which the protons were normally captured by a glass NBO and either bound there or transferred to another surface NBO, sometimes with the participation of water molecules mediating the proton transfer, in a hopping mechanism similar to the one discussed before and shown in Figure 4. The trajectory at 300 K was analyzed in the same way as before, in order to highlight the structural effect of the Na^+/H^+ exchange. The z profile of atomic fractions (panel a in Figure 9), to be compared with the corresponding profile for the nonexchanged surface plotted in Figure 5a, shows that removal (exchange) of Na^+ ions results in a moderate expansion of the surface region, with the surface O atoms protruding further toward the interface, and in a more marked penetration of water within the glass, as denoted by the small peak at $z = 4$ Å in the water density profile (Figure 9b). Removal of Na^+ must be balanced by corresponding interactions, effectively resulting in a more marked interaction between water and Ca^{2+} in the Na/H-exchanged surface. In fact, the rdf's in the bottom panel of Figure 10 for the water molecules in direct contact with the Na-exchanged surface (DHW, $3 < z < 8.7$ Å), represented as bold lines, no longer feature a Na−O_w peak, now replaced by a Ca−O_w peak much more substantial than that in the non-exchanged surface (see Figure 6). The water coordination

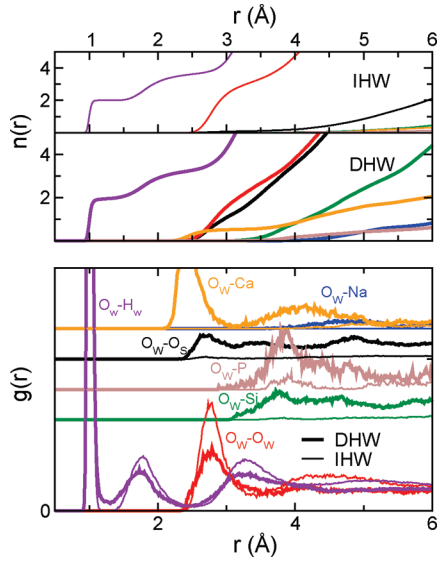

FIGURE 10. Intermolecular rdf's for the Na^+/H^+-exchanged interface. (bottom panel) Intermolecular rdf's for the interaction of water oxygen atoms O_w with O_w and H_w, as well as with O, Si, Na, Ca, and P species of the glass. The rdf's for water molecules in direct contact with the surface (DHW, bold curves) and for those immediately above (IHW, thin curves) are plotted separately. Curves are shifted vertically for clarity. (central and top panels) Cumulative coordination numbers *n(r)*, integrals of the corresponding rdf's in the bottom panel. The central panel shows the *n(r)*'s for water molecules in close contact with the surface (DHW region), whereas the top panel concerns the IHW molecules in the region immediately above.

numbers (central and top panels of Figure 10) indicate that the coordination shell of a water molecule adsorbed at the ion-exchanged interface is composed of 2.7 other water molecules (1.2 donating and 1.5 accepting Hb's), 0.6 Ca^{2+}, and 1.3 surface O atoms: the latter number (compared to 0.5 in the nonexchanged surface) highlights that, besides enabling stronger Ca–water interactions, Na^+ release also results in enhanced surface hydrophilicity, at least partially because of the additional silanol groups formed upon Na/H exchange. The small but significant increase in the Si–O_w coordination number is likely also related to the interaction of water with silanols. The Na^+ removal does not affect the water–water Hb network: similar O_w–O_w and O_w–H_w distances and coordination numbers are recorded in the DHW region of both exchanged and nonexchanged surfaces; stronger water–water Hb's still characterize the DHW region in the exchanged surface model. The fact that each water molecule in the DHW region of the Na-depleted surface is coordinated to a much greater number of surface O atoms suggests that the high affinity of water for Na^+, together with the large availability of these species in the as-created surface, somewhat prevents water from interacting directly with the phosphosilicate glass network: more direct water–network interactions can be established only upon Na release. The structural and chemical changes on the glass surface induced by Na/H exchange do not apparently modify the reactivity of small rings, which remain closed during the (overall) 14 ps of the new MD trajectory.

4. DISCUSSION

In the present simulations, we have used ab initio methods to investigate the dynamics of a realistic model of the BG surface immersed in an extended aqueous environment: the physicochemical effects of the interaction with liquid water were analyzed to characterize specific surface sites, such as small rings, NBOs, and Na^+ or Ca^+ cations. Compared to pure silica, the presence of Na and Ca species alters the physical and chemical properties of the surface in several ways: these species introduce a high fragmentation of the glass network (6, 21), which is reflected in an open and flexible surface structure; moreover, they can directly participate as Lewis acids in the surface adsorption process, as shown by recent spectroscopy/microcalorimetric/modeling studies (62). The present simulations highlighted three main features, which characterize the bioglass surface and whose effects are discussed in detail in the following: (i) initial surface enrichment in Na^+ following immersion; (ii) water dissociation at NBO sites, favored by surface modifier cations; (iii) resistance of 2M rings to hydrolytic opening.

4.1. Initial Enrichment in Na^+. The simulations show that the fragmentation of the silicate network allows water molecules to penetrate the surface without having to break, distort, or even strongly interact with siloxane (Si–O–Si) bonds: in fact, despite the low affinity of water for the siloxane portions of the surface, highlighted in the previous work (40, 46, 63, 64) and confirmed by the present simulations, it is the stronger hydrophilicity of the network-modifier cations that allows molecular water to initially bind to the BG surface and then find access to the inner regions. Compared to the bulk glass, where each Na (Ca) is coordinated to 5–6 glass O atoms (19), water enters the coordination shells of each surface Na^+ and Ca^+ cation to a significant extent, replacing approximately half of the sites in the pseudo-octahedral shell of the cation. The present model of the 45S5 Bioglass(R) surface denotes an initial enrichment in Na species near the top, in agreement with other models of soda-lime silicate surfaces (59, 65). The Na enrichment is such that the glass–water contact immediately establishes dominant Na^+–water interactions in the top region of the 45S5 surface (Figures 5a and 6), which are likely instrumental in the penetration of water beneath the surface, also highlighted in Figure 5a. Sodium is generally not deemed to play a major role in melt-derived BGs: it is added mainly to reduce the melting point of the initial mixture, and Na^+-free compositions can still induce HAp deposition and lead to bone bonding (7). The present results show for the first time that Na–water interactions dominate in the earliest stages of the bioactive process and can effectively start degradation of the surface, before leading to proton exchange and release of Na^+ ions in solution, in a well-established stage of the bioactive mechanism of Hench's glasses (7). Upon Na release, the situation changes: we have created a model of the Na-depleted surface, showing how the hydrophilicity of the surface is further enhanced in this system, because of both the formation of new silanol groups and the higher fraction of Ca^{2+} now found in the top region

(65): in fact, Ca^{2+}—water interactions at BG surfaces can be very strong (29, 34, 62), but the higher fraction of Na^{+} cations that populates the exposed surface of the glass does not allow Ca—water interactions to take place until after most Na is leached.

4.2. NBO Protonation Induced by Modifier Cations. The surface Lewis acidity of Na and Ca modifier cations can provide dissociative pathways for chemisorption of polar molecules, such as water and methanol (29, 62): the present CPMD trajectories show that exposed NBOs can be protonated through water dissociation, provided that the local Lewis acidity can neutralize the remaining OH^{-}. This Lewis acidity can be efficiently provided by *groups* of modifier cations: structures with the hydroxyl group lying at the center of the triangle formed by three cations turn out to be particularly stable, and their formation was often observed following NBO protonation; from this perspective, the high fraction of modifier cations in BG compositions favors this hydroxylation mechanism. An alternative mechanism to neutralize the local negative charge produced by water dissociation at an NBO involves a concerted sequence of proton hoppings along a chain of water molecules, which essentially transfers the OH^{-} "defect" to another region. It is likely that the balance between the two hydroxylation mechanisms depends on the modifier cation concentration and, therefore, on the glass composition. Our results suggest that the high concentration of NBOs strongly associated with charge-balancing modifier cations will trigger water dissociation and NBO protonation in an aqueous fluid, resulting in a significant surface density of OH^{-} groups on most BGs, such as 45S5. A local negative charge on the glass surface is, in fact, considered highly effective for apatite formation, because of its ability to attract further Ca ions from the solution and start deposition of calcium phosphate (38, 66, 67).

4.3. Low Reactivity of 2M Rings. Small phosphosilicate rings are an important feature of the surface of 45S5 BG: as shown by the reconstruction of as-created surface samples in the present and previous ab initio slab models (34), the formation of 2M and 3M rings provides a convenient route to saturate undercoordinated Si and P species always present in the freshly fractured surface of the glass. It is possible that different relaxation mechanisms may dominate in other less bioactive or bioinactive compositions with a higher silica fraction, resulting, for instance, in a lower surface density of small rings: new simulations of the surface of different glass compositions could quantitatively confirm this hypothesis and further substantiate theories where these rings play a key role in the bioactive mechanism (38). In any event, because their presence on the surface appears confirmed at least for the most bioactive compositions (59), a crucial task is to assess their chemical activity using in situ probes (41): in particular, it is interesting to study the effect of exposure of these sites to an aqueous solution at room temperature, in order to assess the form in which they could be available to support further surface processes (nucleation, growth, and crystallization) in the bioactive mechanism (5). The CPMD trajectories highlighted the kinetic stability of 2M rings exposed at the glass surface in contact with liquid water at room temperature: this reflects the kinetic barrier to ring opening through water dissociation, previously calculated for the water monomer (34); while it is much more difficult to evaluate the exact reaction barrier in an extended solid—liquid interface such as the one studied in this work, the room temperature dynamics suggests that the adsorption of multiple water molecules does not remove the barrier: no spontaneous (barrierless) opening of small rings was observed in these systems at room temperature. Instead, as the simulations of a water dimer/trimer interacting with a 2M ring have already been shown, a more favorable chemisorption pathway involves water dissociation *without* ring opening, creating a new surface site where silanol and hydroxyl groups accompany the stable ring. In practice, on a much longer time scale than what can be approached using computer simulations, it is possible that the barrier can be overcome and some of the exposed rings can be opened upon contact with liquid water; however, the clear preference for alternative water dissociation paths highlighted by the present calculations supports the possibility that a fraction of the small rings initially present on the fractured surface will survive in the solid—liquid interface (possibly accompanied by OH^{-} groups coordinated to network-modifier cations as discussed before) for the time sufficient to promote specific processes, such as nucleation of calcium phosphate from the solution (38). The lower reactivity of 2M rings in BG surfaces, compared with the fast hydrolysis of analogous defects in pure silica surfaces (68), results from two factors: (i) the presence in the BG surface of significant amounts of modifier cations and NBO centers, which are more hydrophilic than the siloxane bonds in the 2M ring and displace water molecules away from the ring sites; (ii) the open and therefore more flexible structural arrangement of the BG surface enables a better structural relaxation around the 2M-ring sites, which turn out to be more stable with respect to those found on the amorphous silica surface. The much higher network connectivity of the latter does not allow local relaxation and introduces a much higher tension in the 2M rings, which reduces the kinetic barrier to ring opening (45).

5. FINAL REMARKS

In summary, even though the short time scale of ab initio MD simulations does not enable us to directly model critical processes such as the detachment and dissolution of silicate units into the solution, or the deposition and crystallization of calcium phosphates on the BG surface, the present simulations did provide insight into the structural and dynamical features of the BG—water interface, which affect the above processes. The interaction of water with the as-created BG surface is rather strong because of the presence of basic sites, such as NBOs, and of acidic sites, such as Na (especially in the initial stages of the hydration process) and Ca (69). The observation that water molecules initially associated in dimer and trimers prefer to bind to different regions of the surface rather than to each other seems to denote stronger water—surface interactions than water—

water interactions: overall, the BG surface is hydrophilic, although open patches with a lower siloxane and a higher modifier cation density show a much more marked affinity for water than the phosphosilicate network itself. Besides undercoordinated Si, a small amount of which can always be present and immediately hydroxylated on BG surfaces, NBOs associated with Na/Ca cations appear as the strongest surface sites, able to induce barrierless water dissociation and formation of silanol groups accompanied by hydroxyl groups on the surface. These SiOH−MOH sites, and the corresponding negative charge at physiological pH, appear to play a critical role in the surface reactivity of BGs, together with small silica rings, characterized by a higher kinetic stability compared to the same sites in the pure silica surface, which protects (at least a fraction of) these rings against hydrolytic opening.

Acknowledgment. We thank Devis Di Tommaso (University College London) for providing an equilibrated "CPMD" configuration of liquid water. A.T. thanks the U.K.'s Royal Society for financial support (University Research Fellowship). Computer resources on the HPC*x* and HECToR national supercomputing services were provided via the U.K.'s HPC Materials Chemistry Consortium and funded by EPSRC (Grants EP/D504872 and EP/F067496/1).

REFERENCES AND NOTES

(1) Hench, L. L.; Andersson, O. H. In *An Introduction to Bioceramics*; Hench, L. L., Wilson, J., Eds.; World Scientific: Singapore, 1993.
(2) Hench, L. L. *Science* **1984**, *226*, 630.
(3) Hench, L. L.; Polak, J. M. *Science* **2002**, *295*, 1014.
(4) Vallet-Regi, M.; Ragel, C. V.; Salinas, A. J. *Eur. J. Inorg. Chem.* **2003**, 1029.
(5) Cerruti, M.; Sahai, N. *Rev. Mineral. Geochem.* **2006**, *64*, 283.
(6) Tilocca, A. *Proc. R. Soc. A* **2009**, *465*, 1003.
(7) Hench, L. L. *J. Am. Ceram. Soc.* **1998**, *81*, 1705.
(8) Ebisawa, Y.; Kokubo, T.; Ohura, K.; Yamamuro, T. *J. Mater. Sci.: Mater. Med.* **1990**, *1*, 239.
(9) Vogel, M.; Voigt, C.; Gross, U. M.; Muller-Mai, C. M. *Biomaterials* **2001**, *22*, 357.
(10) Fujibayashi, S.; Neo, M.; Kim, H.-M.; Kokubo, T.; Nakamura, T. *Biomaterials* **2003**, *24*, 1349.
(11) Lebecq, I.; Desanglois, F.; Leriche, A.; Follet-Houttemane, C. *J. Biomed. Mater. Res., Part A* **2007**, *83*, 156.
(12) Xin, R. L.; Leng, Y.; Chen, J. Y.; Zhang, Q. Y. *Biomaterials* **2005**, *26*, 6477.
(13) Knowles, J. C. *J. Mater. Chem.* **2005**, *13*, 2395.
(14) Levy, S.; Van Dalen, M.; Agonafer, S.; Soboyejo, W. O. *J. Mater. Sci.: Mater. Med.* **2007**, *18*, 89.
(15) Leonova, E.; Izquierdo-Barba, I.; Arcos, D.; Lopez-Noriega, A.; Hedin, N.; Vallet-Regi, M.; Eden, M. *J. Phys. Chem. C* **2008**, *112*, 5552.
(16) Martin, R. A.; Salmon, P. S.; Carroll, D. L.; Smit, M. E.; Hannon, A. C. *J. Phys.: Condens. Matter* **2008**, *20*, 115204.
(17) FitzGerald, V.; Pickup, D. M.; Greenspan, D.; Sarkar, G.; Fitzgerald, J. J.; Wetherall, K. M.; Moss, R. M.; Jones, J. R.; Newport, R. J. *Adv. Funct. Mater.* **2007**, *17*, 3746.
(18) Moss, R. M.; Pickup, D. M.; Ahmed, I.; Knowles, J. C.; Smit, M. E.; Newport, R. J. *Adv. Funct. Mater.* **2008**, *18*, 634.
(19) Tilocca, A.; de Leeuw, N. H. *J. Phys. Chem. B* **2006**, *110*, 25810.
(20) Mead, R. N.; Mountjoy, G. *J. Phys. Chem. B* **2006**, *110*, 14273.
(21) Tilocca, A.; Cormack, A. N.; de Leeuw, N. H. *Chem. Mater.* **2007**, *19*, 95.
(22) Tilocca, A.; Cormack, A. N.; de Leeuw, N. H. *Faraday Discuss.* **2007**, *136*, 45.
(23) Tilocca, A. *Phys. Rev. B* **2007**, *76*, 224202.
(24) Tilocca, A.; Cormack, A. N. *J. Phys. Chem. B* **2007**, *111*, 14256.
(25) Tilocca, A. *J. Chem. Phys.* **2008**, *129*, 084504.
(26) Tilocca, A.; Cormack, A. N. *Nuovo Cimento B* **2008**, *123*, 1415.
(27) Greaves, G. N. *J. Non-Cryst. Solids* **1985**, *71*, 203.
(28) Ramila, A.; Vallet-Regi, M. *Biomaterials* **2001**, *22*, 2301.
(29) Cerruti, M.; Magnacca, G.; Bolis, V.; Morterra, C. *J. Mater. Chem.* **2003**, *13*, 1279.
(30) Kinney, D. R.; Chuang, I.; Maciel, G. E. *J. Am. Chem. Soc.* **1993**, *115*, 6786.
(31) Fois, E.; Gamba, A.; Tabacchi, G.; Coluccia, S.; Martra, G. *J. Phys. Chem. B* **2003**, *107*, 10767.
(32) Marx, D.; Hütter, J. In *Modern Methods and Algorithms of Quantum Chemistry*; Grotendorst, J., Ed.; NIC Series 301; John von Neumann Institute for Computing: Jülich, Germany, 2000; Vol. 1.
(33) Car, R.; Parrinello, M. *Phys. Rev. Lett.* **1985**, *55*, 2471.
(34) Tilocca, A.; Cormack, A. N. *J. Phys. Chem. C* **2008**, *112*, 11936.
(35) Geissberger, A. E.; Galeener, F. L. *Phys. Rev. B* **1985**, *28*, 3266.
(36) Wallace, S.; West, J. K.; Hench, L. L. *J. Non-Cryst. Solids* **1993**, *152*, 101.
(37) Hench, L. L.; West, J. K. *Annu. Rev. Mater. Sci.* **1995**, *25*, 37.
(38) Sahai, N.; Anseau, M. *Biomaterials* **2005**, *26*, 5763.
(39) Tilocca, A.; Selloni, A. *J. Phys. Chem. B* **2004**, *8*, 19314.
(40) Bolis, V.; Fubini, B.; Marchese, L.; Martra, G.; Costa, D. *J. Chem. Soc., Faraday Trans.* **1991**, *87*, 497.
(41) Cerruti, M.; Morterra, C.; Ugliengo, P. *Chem. Mater.* **2005**, *17*, 1416.
(42) Hass, K. C.; Schneider, W. F.; Curioni, A.; Andreoni, W. *Science* **1998**, *282*, 265.
(43) Odelius, M. *Phys. Rev. Lett.* **1999**, *82*, 3919.
(44) Tilocca, A.; Selloni, A. *J. Phys. Chem. B* **2004**, *8*, 4743.
(45) Rimola, A.; Ugliengo, P. *J. Chem. Phys.* **2008**, *128*, 204702.
(46) Iler, R. K. *The Chemistry of Silica*; Wiley: New York, 1979.
(47) Legrand, A. P. *The Surface Properties of Silica*; Wiley: New York, 1998.
(48) Giannozzi, P.; et al. http://www.quantum-espresso.org.
(49) Perdew, J. P.; Burke, K.; Ernzerhof, M. *Phys. Rev. Lett.* **1996**, *77*, 3865.
(50) Vanderbilt, D. *Phys. Rev. B* **1990**, *41*, 7892.
(51) Masini, P.; Bernasconi, M. *Phys. Rev. B* **2002**, *14*, 4133.
(52) Rignanese, G.-M.; Charlier, J.-C.; Gonze, X. *Phys. Chem. Chem. Phys.* **2004**, *6*, 1920.
(53) Mischler, C.; Horbach, J.; Kob, W.; Binder, K. *J. Phys.: Condens. Matter* **2005**, *17*, 4005.
(54) Fois, E.; Gamba, A.; Tilocca, A. *J. Phys. Chem. B* **2002**, *106*, 4806.
(55) Tilocca, A.; Selloni, A. *J. Chem. Phys.* **2003**, *119*, 7445.
(56) Adeagbo, W. A.; Doltsinis, N. L.; Klevakina, K.; Renner, J. *ChemPhysChem* **2008**, *9*, 994.
(57) Tilocca, A.; Selloni, A. *ChemPhysChem* **2005**, *6*, 1911.
(58) Tilocca, A.; Di Valentin, C.; Selloni, A. *J. Phys. Chem. B* **2005**, *109*, 20963.
(59) Zeitler, T. R.; Cormack, A. N. *J. Cryst. Growth* **2006**, *294*, 96.
(60) Ma, Y.; Foster, A. S.; Nieminen, R. M. *J. Chem. Phys* **2005**, *122*, 144709.
(61) Note that the absolute values of the calculated water densities $\rho(z)$ should be considered as only indicative, because of the small volume of each z slice, but their relative trend is more representative.
(62) Bolis, V.; Busco, C.; Aina, V.; Morterra, C.; Ugliengo, P. *J. Phys. Chem. C* **2008**, *112*, 16879.
(63) Grabbe, A.; Michalske, T. A.; Smith, W. L. *J. Phys. Chem.* **1995**, *99*, 4648.
(64) Hassanali, A. A.; Singer, S. J. *J. Phys. Chem. B* **2007**, *111*, 11181.
(65) Corrales, L. R.; Du, J. *J. Am. Ceram. Soc.* **2006**, *89*, 36.
(66) Li, P.; Yang, Q.; Zhang, F.; Kokubo, T. *J. Mater. Sci.: Mater. Med.* **1992**, *3*, 452.
(67) Cho, S. B.; Miyiaji, F.; Kokubo, T.; Nakanishi, K.; Soga, N.; Nakamura, T. *J. Mater. Sci.: Mater. Med.* **1998**, *9*, 279.
(68) Bunker, B. C.; Haaland, D. M.; Michalske, T. A.; Smith, W. L. *Surf. Sci.* **1989**, *222*, 95.
(69) Even though the number/distribution of reactive sites on the surface could change for differently prepared samples, the water adsorption properties of specific surface sites, such as NBOs, modifier cations, and small rings, are hardly affected when different fractions of these sites are present.

AM900198T